

# Tele-Impedance: Towards Transferring Human Impedance Regulation Skills to Robots

A. Ajoudani, N. G. Tsagarakis and A. Bicchi

**Abstract**—This work presents the novel concept of Tele-Impedance as a method for controlling/teleoperating a robotic arm while performing tasks which require significant dynamics variation. As an alternative method to bilateral force-reflecting teleoperation control approach, which uses a position/velocity command combined with force feedback from the robot side, Tele-Impedance enriches the command sent to the slave robot by combining the position reference with a stiffness (or full impedance) reference estimated from the arm of the human operator. We propose a new method to estimate the stiffness of the human arm based on the agonist-antagonist muscular co activations. The concept of the Tele-Impedance is demonstrated using the KUKA light weight robotic arm as the slave manipulator in a ball reception experiment. The performance of Tele-Impedance control method is assessed by comparing the results obtained while receiving the ball, with the slave arm under i) constant low stiffness, ii) constant high stiffness or iii) under Tele-Impedance control. Performance indexes are defined and used for the comparative study of the ball reception performances under the different endpoint elastic profiles. The experimental results demonstrate the effectiveness of the task-related Tele-Impedance control method and highlight its potential use to execute tasks which require significant dynamics variation.

## I. INTRODUCTION

Transferring the stability and versatile skills of human interaction behavior in robots is a major concern in robotics. Bio-signals such as electromyography (EMG) and electroencephalography (EEG) have been widely used as controller inputs for robots, prosthetic devices and exoskeletons encapsulating information about the kinematics and dynamics of performed action [1-3] and demonstrating high efficiency [4, 5] due to their availability, stability and fast adaptation.

Concentrating on human arm and tasks requiring dynamics variation or being exposed to mechanical disturbances, the contact reliability can be explained by considering a stable mechanical interface between human arm endpoint and the environment [1, 6-8, 21]. Central nervous system (CNS) is deemed to have the ability to adapt and learn goal dependant kinematic and dynamic models of the external world [9]. However, previous results suggest the

existence of a separate mechanism for incorporation of the inverse dynamic models (for the joint torque modifications) and impedance control, while interacting with environments with uncertainties and stochastic disturbances [6]. The former is carried out by selective changes in patterns of activations in individual muscles in order to generate task-efficient force at the contact level while the latter is conducted by synchronized agonist-antagonist muscle cocontractions without causing any force fluctuations at contact level. This task-dependant impedance modification meets necessities for increased stability, accuracy and task readiness [1-2, 6 and 19].

Incorporation of noted exclusive mechanical properties in robotic arms will increase stability of their behavior while exposed to mechanical instabilities. In the past decade, the introduction of torque controlled robots which can regulate actively their stiffness or full impedance properties by active control techniques [10] as well the recent developments of actuation systems which inherently integrate physical principles such as variable stiffness and damping [11-13] have increased the potential of porting the human skills in robotic and assistive devices in terms of safety, performance and stability [11].

A method for mapping exclusive features of human action to robot side is teleoperation. The execution of the remotely performed task is usually assisted by feeding back to the master and human operator kinesthetic feedback related to the interaction forces between the slave robot and the remote environment. Although these bilaterally controlled teleoperated systems outperform the pure position controlled systems, latencies in communication may still generate serious stability issues [14-16]. Despite the progress made in the control and the stability of bilateral controlled teleoperation systems, there are still many tasks in which stability and reduced transparency, if not mere cost of sensing and actuating reflected forces, prevents application of bidirectional teleoperation. Tasks which are normally performed by humans without difficulty such as drilling, reaming, chipping and many others with large uncertainty in the environment constraints, cannot be easily conducted under teleoperation control. This is not only due to the stability and transparency issues mentioned above but also in many cases due to inadequate or low quality sensory information (such as position, force, velocity) which defines the mechanical work exchanged during the interaction between end effector and the remote environment [17].

The interaction performance of the human arm achieved through the regulation of its endpoint impedance and by

A. Ajoudani and A. Bicchi are with Interdepartmental Research Centre “E. Piaggio”, Faculty of Engineering, University of Pisa, and with the Dept. of Advanced Robotics, Istituto Italiano di Tecnologia, Via Morego 30, 16163, Genova, Italy (e-mails: arash.ajoudani@iit.it and bicchi@centropiaggio.unipi.it).

N. G. Tsagarakis is with the Dept. of Advanced Robotics, Istituto Italiano di Tecnologia, Via Morego 30, 16163, Genova, Italy (e-mails: nikos.tsagarakis@iit.it).

means of muscular coactivations and the optimal endpoint path trajectories descending from CNS for path plannings is very effective. Inspired by this observation, Tele-Impedance control as an alternative method to unilateral position based control or bilateral force reflecting control is proposed during teleoperated tasks which require significant dynamics variation. The novelty of the proposed Tele-Impedance control method is that it provides the robot with task-related elastic profile in addition to position trajectories. This combined reference command (position and impedance) is finally executed by the slave teleoperated robotic arm by means of accurate local controllers [10]. In this work, the efficiency of the Tele-Impedance algorithm is evaluated in ball reception experiments. On the master side, the subject is performing the ball catching task while on the remote side, the robotic arm is performing simultaneously the same task while copying the kinematics and elastic profile modifications of the human's endpoint in real time. The performance of the proposed algorithm is compared to different constant profiles of the robot's endpoint according to defined performance indexes.

The paper is structured as follows; section II presents the estimation of human arm impedance in 3D space and the identification-calibration process. Section III presents the experimental setup used for the execution of the catching the ball task using the Tele-Impedance control. Experimental results for the stiffness estimation as well as data from the execution of task using the Tele-Impedance concept are introduced in section IV. Finally section V addresses the conclusions.

## II. HUMAN ARM IMPEDANCE ESTIMATION IN 3D

### A. Co-Constrictions Based Index of Endpoint Stiffness

Task-efficient modifications of the endpoint arm impedance along with endpoint force fluctuations in humans are shown to have high correlations with the patterns of activations in involved muscles [1, 6-8]. Agonist-antagonist muscle co-contractions are deemed to affect and modify selectively the overall stiffness and viscous profiles of the arm endpoint, decoupled from force fluctuations. This exclusive feature enables the human arm to perform versatile and stable movements while interacting with environments with uncertainties and stochastic disturbances [6].

Endpoint force fluctuations and impedance adjustments can be regarded as internal force regulations exerted by group of extensor and flexor muscles. For instance, simultaneous increase in tension of flexor and extensor muscles will modify impedance at joint and endpoint level without causing any joint or endpoint force fluctuations. On the other hand, based on high correlation between surface EMG and generated muscle tension, the proposed model in [1] will account for the endpoint force changes due to variations in patters of activations in corresponding muscles (Eq. 1).

$$\begin{bmatrix} f_{ex} \\ f_{ey} \\ f_{ez} \end{bmatrix} = \mathbf{T} \begin{bmatrix} P_{flex1} \\ \vdots \\ P_{ext4} \end{bmatrix} \quad (1)$$

Here,  $f_{ex}$ ,  $f_{ey}$  and  $f_{ez}$  denote the generated forces at the human arm endpoint in x, y and z directions, respectively.  $P_{flex}$  and  $P_{ext}$  are pre-processed flexor and extensor EMG signals (four flexor-extensor pairs), and  $\mathbf{T}: \mathfrak{R}^8 \rightarrow \mathfrak{R}^3$  symbolizes the linear mapping to be estimated. Components of this mapping incorporate information such as the moment arm, conversion factor from muscle activity to muscle tension and Jacobian coefficients of the transformation kinematics. They are therefore arm configuration dependent.

Based on the independency of the two subsystems described above, muscular activities can be then decomposed and mapped into two subspaces. First mapping corresponds to the force fluctuations and the second will be defined as the kernel of the former which correlates of impedance regulations without causing any effect on generated joint/endpoint forces:

$$\mathbf{F} = \mathbf{T}(\mathbf{P} + \mathbf{N}_T \mathbf{P}) \quad (2)$$

where  $\mathbf{F}$  is the force vector defined in Eq.1 and  $\mathbf{N}_T = \left\{ \mathbf{P}_{null} \in \mathfrak{R}^8 : \mathbf{T} \mathbf{P}_{null} = \vec{0} \right\}$  denotes the kernel (null-space) of the EMG-to-Endpoint force transformation and is defined by:

$$\mathbf{N}_T = \mathbf{I} - \mathbf{T}^T (\mathbf{T} \mathbf{T}^T)^{-1} \mathbf{T} \quad (3)$$

where  $\mathbf{I} \in \mathfrak{R}^{8 \times 8}$  is the identity matrix and  $\mathbf{T}^T$  denotes the transformation of the  $\mathbf{T}$  matrix. Standing on above formulations, the overall muscular activities can be decomposed to force related and null-space (co-activation based internal force fluctuations) sub inputs:

$$\mathbf{P} = (\mathbf{T}^+ \mathbf{T}) \mathbf{P} + \overbrace{(\mathbf{I} - \mathbf{T}^+ \mathbf{T}) \mathbf{P}}^{\mathbf{P}_{null}} \quad (4)$$

where  $\mathbf{T}^+ = \mathbf{T}^T (\mathbf{T} \mathbf{T}^T)^{-1}$ . The second part of above equation is related with the portion of muscular activities which are independent from endpoint force fluctuations.

Spring like behavior of the human arm muscles provides intrinsic endpoint impedance properties which could be represented by corresponding ellipsoids. Concerning its elastic behavior, the orientation of this ellipsoid in endpoint is highly posture dependant and the size (area of the ellipse) changes by the level of co-activation of the muscles [1, 6, and 7]. Based on these facts, three major axes of ellipsoid can be defined by a constant part which states the intrinsic elastic properties of the human endpoint and a variable part according to muscular co-activations:

$$\mathbf{K}_{end} = \mathbf{K}_{posture} + \mathbf{\Psi} \mathbf{P}_{null} \quad (5)$$

where  $\mathbf{K}_{end} \in \mathfrak{R}^3$  and  $\mathbf{K}_{posture} \in \mathfrak{R}^3$  represent the endpoint and intrinsic posture dependant endpoint stiffness matrices in Cartesian space, respectively; and  $\mathbf{\Psi}: \mathfrak{R}^8 \rightarrow \mathfrak{R}^3$  denotes the

mapping from resulting null-space transformation of muscular activities, to additional (co-activation based) endpoint stiffness values in three major directions in Cartesian space. The overall block diagram of Tele-Impedance control scheme is shown in Fig. 1.

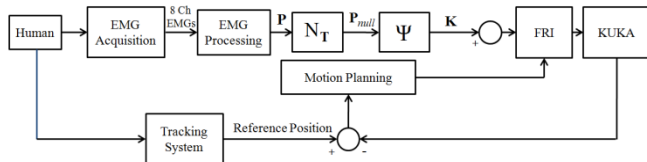


Fig. 1. The overall block diagram of Tele-Impedance.

The generalization of the above transformations within the arm workspace will not be valid due to nonlinear dependency of the muscular activity and generated muscle tensions especially during movements. However, since the task performed by human arm and mimicked by the robot will be accomplished in the vicinity of the isometric posture in which the parameters are estimated and calibrated in 3D (based on two different experimental protocols described below), the overall approach can provide us with the insightful outline of the generated endpoint stiffness profile. In addition, proposed algorithm prioritizes position accuracy through a closed-loop and robust position control algorithm using accurate position tracking system.

### B. Stiffness Index Model and Null-Space Transformation Calibrations

One healthy subject (male; age 27) participated in identification-calibration and catching the ball experiments. The subject stood upright with the feet side-by-side and his shoulder to shoulder line along the x axis of the robot's reference frame. In this arrangement the subject interacted with the KUKA light weight robotic arm (KUKA/DLR) in force regulation and random perturbation experiments. A spherical joint were designed, fabricated and mounted to the endpoint of KUKA in order to reduce undesired generated torques by the subject's wrist (Figure 2. B). The end effector of the KUKA arm was equipped with a 6 axis force-torque sensor (ATI-Mini-45). The subject was asked to apply constant forces [5, 10 and 20N] along 6 directions [ $\pm x$ ,  $\pm y$  and  $\pm z$ ] while holding the handle under isometric conditions. Each trial was 60 seconds long from which the first 10 seconds was not used for the processing described below due to transient force fluctuations. For each direction and force level, 4 trials (total of  $4 \times 6 \times 3$  trials) were recorded for the purpose of the model calibration.

During the execution of these trials, EMGs from eight flexor/extensor muscles (Table .1 and Figure 2. A) were acquired by means of surface electrodes (Delsys-Bangoli-16 from (Delsys Inc.)). The signals were filtered [Band-pass, 20 Hz (low) and 450 Hz (high)], sampled at 2 KHz (PCI-6220, National Instruments) and full rectified. A digital non-causal FIR linear phase low-pass filter was used for the detection of the envelope of the signal, which approximately corresponds to muscle activity. Least square error optimization algorithm was recruited for the identification of model parameters, Eq. (1). After the disintegration of the EMGs to

the generated force values in 3 different directions, the parameters were identified and used as a first step for the calibration process.

TABLE I  
MUSCLES ACCOUNTED FOR EMG MEASUREMENTS

Flexors		Extensors	
Monoarticular	Biarticular	Monoarticular	Biarticular
Deltoid calvaric part (DELC)	Biceps long head (BILH)	Deltoid scapular part (DELS)	Triceps long head (TRIO)
Pectoralis major calvaric part (PMJC)		Triceps lateral head (TRIA)	
Brachioradialis (BRAD)		Triceps medial head (TRIM)	

In order to have an insight for the accuracy of the optimization, Pearson's product-moment correlation coefficient which measures the strength of linear dependency of the estimated and measured force signals was used for the calculation of coefficient of determination. The later parameter describes the proportion of the variance of measured and the estimated force signals from eight EMG measurements.

$$r_{pearson\ k} = \frac{\sum f_k \cdot \hat{f}_k - \frac{\sum f_k \sum \hat{f}_k}{N}}{\sqrt{(\sum f_k^2 - \frac{(\sum f_k)^2}{N})(\sum \hat{f}_k^2 - \frac{(\sum \hat{f}_k)^2}{N})}} \quad (6)$$

$$R_k^2 = (r_{pearson\ k})^2$$

where  $r$  and  $R^2$  are the correlation coefficient and coefficient of determination, and  $f$  and  $\hat{f}$  are the measured and estimated force values, respectively. A second set of experiments was carried out to further calibrate the stiffness index model by means of real measurements of human arm endpoint impedance in four levels of muscular cocontractions (minimum and three levels of co-contractions).

Extensive literature exists on the estimation of human arm endpoint stiffness from the steady-state force response of the human arm to step-like and other similar position perturbations [6, 8 and 19]. Priory assumptions concerning the linearity of the endpoint impedance behavior and undeniable voluntary responses of the subjects under perturbed experiments have encouraged researchers for the application of random position perturbations to cope with the noted drawbacks [7]. In this work, stochastic perturbations (step-like, 200 msec duration) was applied to the subjects hand, holding the handle, in x, y and z directions. The amplitude of the displacement was between 10 and 20 millimeters. This perturbation pattern will minimize the probability of voluntary reactions due to its random nature. The six axes F/T sensor mounted at the end-effector of the KUKA robotic arm was in charge of monitoring the restoring forces. The overall postures of the subject in both identification/calibration and task (catching the ball) experiments were identical. The displacements of the human arm at the endpoint (level of the wrist) along with shoulder and elbow positions were tracked (resolution: 0.02 mm) by Optitrack system (Natural Point Inc). The interfaces

between the KUKA controller, the EMG acquisition board, the Optitrack position streaming data and the six axes F/T sensor in calibration experiment and real-time Tele-Impedance experiments were developed in C++.

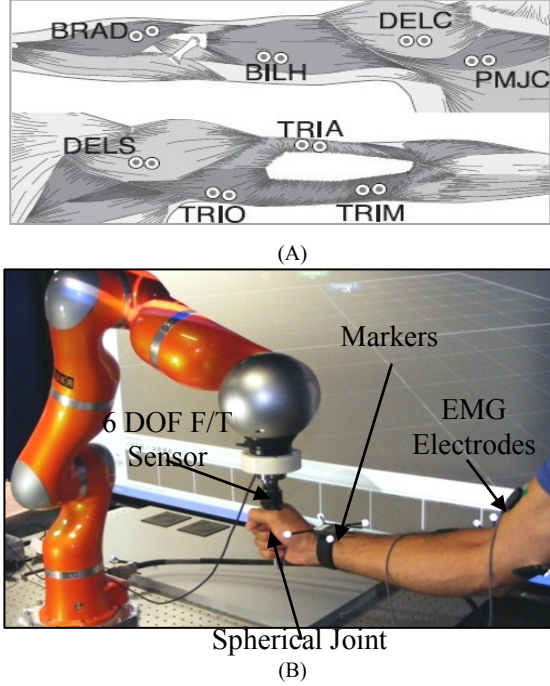


Fig. 2. A. Electrode positions in EMG measurements. B. Experimental setup for the first calibration set of experiments. Subject inserts constant forces in 6 directions while holding the spherical joint. The KUKA robotic arm is not actively interacting in the first set of calibration trials.

The robot's position and the joint or Cartesian stiffness commands were sent to the KUKA controller using the DLR's Fast Research (FR) Interface [18]. The Cartesian stiffness values of KUKA robotic arm were set to the highest values possible for the perturbation experiments. Position and force measurements were performed at a sampling frequency of 200 Hz while the EMG acquisition and processing was performed at a frequency of 1 KHz. All the acquired force/torque and position measurements were filtered [Butterworth, low-pass, cutoff frequency 15 Hz] to eliminate high frequency noise.

Dynamic presentation of the endpoint impedance in human arm and in frequency domain can be described by Eq. (7), where  $F_x(f)$ ,  $F_y(f)$  and  $F_z(f)$  are Fourier transforms of the endpoint force along x, y and z directions, and  $x(f)$ ,  $y(f)$  and  $z(f)$  are the Fourier transforms of the human endpoint displacements. The impedance dynamics between the inserted displacements and corresponding force fluctuations are described by Fourier transforms of the transfer functions ( $G_{ij}$ ) as single input single output subsystems [7]. The idea can be generally described by the possibility of decomposing MIMO system to different linear SISO subsystems. In this work, the resulting SISO linear subsystems were non-parametrically identified in frequency domain.

$$\begin{bmatrix} F_x(f) \\ F_y(f) \\ F_z(f) \end{bmatrix} = \begin{bmatrix} G_{xx} & G_{xy} & G_{xz} \\ G_{yx} & G_{yy} & G_{yz} \\ G_{zx} & G_{zy} & G_{zz} \end{bmatrix} \begin{bmatrix} x(f) \\ y(f) \\ z(f) \end{bmatrix} \quad (7)$$

Considering the sufficiency of a second order linear model for the representation of the endpoint impedance in human arm [7, 8, 19] (based on results to be demonstrated later), the second order linear model, Eq. (8) was fit to each one of SISO transfer functions, where I, B and K assimilate the endpoint inertia, viscosity and stiffness matrices, respectively.

$$G_{ij} = I_{ij}s^2 + B_{ij}s + K_{ij} \quad (8)$$

The resulting transformation in time domain can be restated by the following parameterized model:

$$\mathbf{M}_{EP}\ddot{\mathbf{X}}(t) + \mathbf{B}_{EP}\dot{\mathbf{X}}(t) + \mathbf{K}_{EP}(\mathbf{X}(t) - \mathbf{X}_{eq}) = -\mathbf{F}(t)$$

$$\mathbf{X}(t) = \begin{bmatrix} x(t) \\ y(t) \\ z(t) \end{bmatrix} \quad \text{and} \quad \mathbf{F}(t) = \begin{bmatrix} f_x(t) \\ f_y(t) \\ f_z(t) \end{bmatrix} \quad (9)$$

The experiments were done in four levels of co-contractions. The stiffness index proposed in [1] was used in order to have an intuitive trace of the cocontraction level.

$$\begin{bmatrix} S_{xx} \\ S_{yy} \\ S_{zz} \end{bmatrix} = |\mathbf{T}| \times \mathbf{P} \quad (10)$$

Here,  $S_{xx}$ ,  $S_{yy}$  and  $S_{zz}$  denote endpoint stiffness indexes of the human arm in x, y and z directions and the absolute value of the  $\mathbf{T}$  matrix is meant elementwise. By means of above definitions, Total Co-contraction Index (TCI) is defined and visually fed back to the subject for the purpose of cocontraction level stabilization.

$$TCI = S_{xx} + S_{yy} + S_{zz} \quad (11)$$

The first set of perturbations was applied to the subject's hand in minimum muscle activity levels. The subject was then asked to co-contrast his arm muscles as high as possible. Consequently, three levels of TCI with 10% of allowed deviations were defined based on the minimum-maximum TCI margins. Following this the subject was asked to keep the TCI in the predefined levels, while holding the handle at the KUKA end effector and random perturbations were applied. Five successful trials were recorded for each state of the TCI level. The trial in which variation of the TCI was not exceeded from  $\pm 10\%$  of its defined level was considered successful. The minimum TCI trials were used for the identification of the intrinsic endpoint impedance matrices. Meanwhile, the higher TCI trials were used for the identification and calibration of the additional stiffness values due to raise of null-space mapped EMG's at endpoint level. Based on the presumption for invariant behavior of the endpoint inertia in the vicinity of the predefined posture, the inertial matrix was identified once from the first set of trials (minimum activation). The resulting matrix was applied as constant values for the estimation of endpoint visco-elastic matrices in the rest of higher level co-activation experiments. Each perturbation trial had the duration of 60 seconds where the first 5 seconds were used for the bias removal from the force torque sensor

and subject's adaptation to required TCI levels. At the beginning of 6<sup>th</sup> second, stochastic perturbations applied in six directions as described above. The gravitational force at the end point were considered as bias and removed at the processing part of the trial assuming that they remain constant for small deviations from the equilibrium point.

The stiffness estimated from the minimum muscular activities were assigned as intrinsic endpoint elastic behavior in Eq. (5), corresponding to that specific posture. The coactivation model of the endpoint stiffness,  $\Psi$ , was identified by means of a linear fit from the results of  $\mathbf{P}_{null}$  and the stiffness level identified during the higher TCI trials.

### III. BALL CATCHING EXPERIMENTS

Evaluative study of proposed algorithm was performed by means of catching the ball experiments. Three types of catching experiments were performed in favor of the performance evaluations for different behaviors of endpoint elastic profile in the slave robotic arm. Comparative study was conducted based on performance indexes extracted from transient (bouncing) and steady state (deviation from equilibrium position) behavior. A rigid, bowl shape hand (nonprehensive catching) was fabricated and mounted on the end effector of the KUKA arm after the 6 axes F/T sensor. The experimental setup and data flow are shown in Fig 3. Rigid body markers were attached to the wrist, elbow and shoulder of human arm to track the human's arm motion. However, the only data, used for the motion planning and reference trajectory calculation was the human arm endpoint path (wrist level). The rest of the markers were used to validate if the catching posture during a trial was closely matching to the posture maintained during the identification-calibration experiments. At the same time, EMG signals were acquired for the purpose of the human arm endpoint stiffness calculations based on the procedure described in the previous section. All processing and control algorithms were performed in real-time. Software interfaces, sampling frequencies, and hardware specifications are identical to those reported in the previous sections.

Two similar rigid balls ( $m=0.92\text{kg}$ ,  $\text{radius}=52.5\text{mm}$ ) were thrown synchronously from same distance with respect to the human and robotic arm endpoints. At human side, the subject had the same posture, identical to the identification-calibration experiments. Synchronization of the ball impact in both sides has a very dominant role in evaluation of the results. This was done by ensuring that the free falling distances of the two balls are equal and the two balls were dropped at the same time using a simple release mechanism.

The equilibrium position of the human endpoint before and during catching was mapped to KUKA's endpoint path in all experiments where the Cartesian stiffness values were set to relatively high [1.2, 1.2, 1.2 KN/m], low [120, 120, 120 N/m] and under Tele-Impedance, once at a time. Constant endpoint damping values were chosen for all three experiments even though further extension of the proposed method provides the possibility of transferring the endpoint damping behavior of human to robot side under Tele-Impedance.

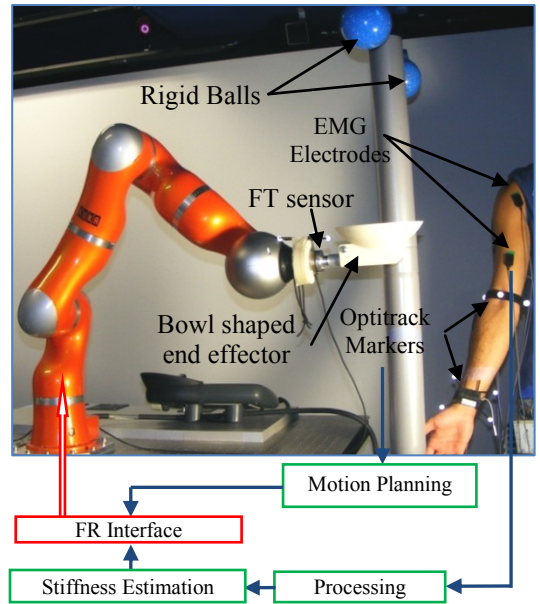


Fig. 3. Experimental setup. KUKA light weight robotic arm, EMG electrodes, position tracking markers and F/T sensor are shown in picture.

*Motion Planning:* KUKA's base frame was considered as the reference frame and all other frames (Optitrack and FT sensor frames) were conformed to this reference frame. The position path of the human wrist was measured, filtered [low-pass, cutoff 15Hz] and used for the trajectory planning.

The FR Interface was utilized for commanding the KUKA arm. Incremental position references were sent to KUKA, calculated from the position tracking errors in three dimensions (Eq. 12). This approach was taken into account to cope with the drift problem and tracking inaccuracy due to any possible delay between reference commands and generated movement in KUKA's end-effector.

$$\mathbf{e}_z = \xi_{human} - \xi_{kuka} \quad (12)$$

where  $\mathbf{e}_z$  is three dimensional tracking error vector between the reference Cartesian position vector of human wrist  $\xi_{human}$ , and the current Cartesian position vector of KUKA's end-effector,  $\xi_{kuka}$ . The details about the local position and impedance controllers in robot's side are described in [10].

*Performance Indexes:* In this work, a comparative analysis of the quality of the reception of the ball is evaluated using the bouncing index (BI) which is computed by the integration of the force values lower than steady state force and after the first impact, over the time. High bouncing index is the result of a reception with multiple bouncing and long under damped ball trajectories. Another index is defined which simply represents the deviation from equilibrium position in z direction at steady state and is defined by:  $PEI = \mathbf{e}_{z,ss}$ . The force ratio between second impact and first one (bouncing force ratio (BFR)), forms the third reception quality index since it provides a measure of the damping action achieved during the ball reception under different stiffness profiles.

#### IV. RESULTS

All components of matrix  $T$  (Eq. 1) were identified by means of least square error algorithm (average  $R^2 = 81\%$  across all force regulation trials). Second order linear models were fit to non parametrically identified transfer functions in the frequency range of  $[0\ 10]$  Hz (Fig. 4). The coefficient of determination ( $R^2$ ) was calculated across all minimum TCI trials (average = 74%). Once all the mappings and model parameters were identified, the ball catching task was performed under different endpoint elastic profiles of the slave robotic arm.

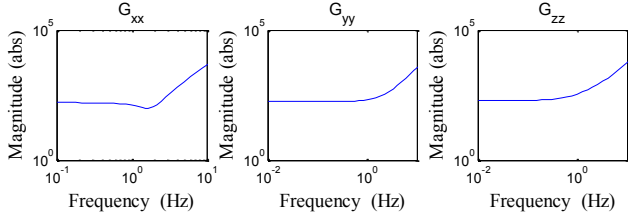


Fig. 4. Estimated second order endpoint impedance transfer functions of  $G_{xx}$ ,  $G_{yy}$  and  $G_{zz}$  by means of stochastic perturbations.

The measured forces and deviation errors from the reference equilibrium position at the endpoint of the slave robotic arm during the task are depicted in Fig. 5 and 6 under different elastic profiles (stiff, compliant and Tele-Impedance). The regulation of the cocontraction levels of human arm muscles and resulting endpoint stiffness modifications during the catching experiment are introduced in Fig. 7. At the beginning of the experiments, small constant increase in muscular activities were observed which led to relatively small increase in endpoint Cartesian stiffness values, compared to minimum TCI trials, which may refer to task readiness impedance modifications [19]. Increased impedance at the moment of impact and its descending behavior after maintained stability are the results of muscular activity regulation by the subject.

As discussed before, CNS is deemed to increase cocontraction levels of shoulder, elbow and biarticular muscles which result in an increased impedance and decreased movement error [20-22]. Some other behavioral studies demonstrate increase of cocontraction levels in human arm while performing tasks which need quick torque generations and/or to cancel components of torques orthogonal to the desired direction [2]. This goal-directed adaptation of the endpoint elastic profile is transferred to KUKA arm in realtime. It means that the endpoint stiffness of the slave robot is commanded to follow the reference values demonstrated in Fig. 7, lower plot.

Transient behavior of the system under Tele-Impedance is benefited from the raised stiffness at the very beginning of the impact ( $t= 2.3$  to  $2.4$  sec) which leads to minimized deviation from reference equilibrium position. The stiffer the arm the smaller the deviation is as it can be seen in experimental results under constant high elastic profile (Fig 6, left plot). The price paid for the accuracy and reduced deviation from equilibrium position due to the higher values of the end point stiffness is the occurrence of the bouncing phenomenon. The second force peak (at  $t = 5.26$  sec) in the

stiff case refers to second impact of the ball as a consequence of the bouncing (Fig. 5, left plot).

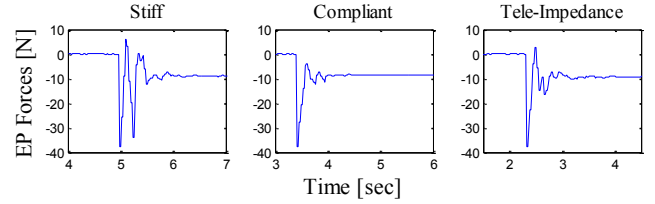


Fig. 5. Measured force values in z direction during the task with the slave robotic arm under stiff, compliant and Tele-Impedance endpoint elastic profile.

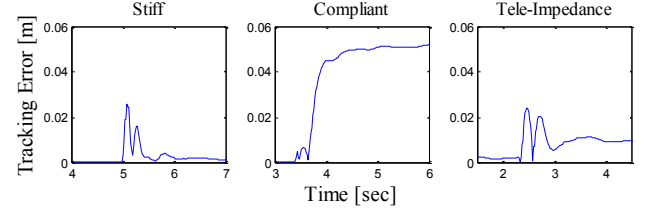


Fig. 6. Absolute tracking position error in z direction during the task with the slave robotic arm under stiff, compliant and Tele-Impedance endpoint elastic profile.

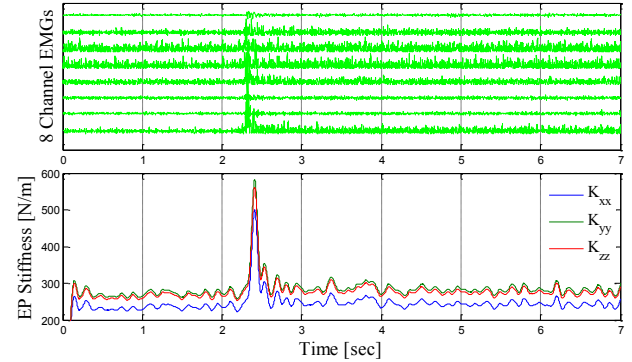


Fig. 7. Full rectified eight channel raw EMGs (upper plot) and estimated and mapped endpoint stiffness (lower plot) in real-time.

One way of course to obtain a stable contact is to reduce the endpoint stiffness values. However, this directly affects the position deviation, especially when endpoint elastic profile behaves under constant low values (compliant case, Fig. 6, mid plot). Other drawback of such compliant profile is the insufficiency to generate torques in repositioning the ball to its equilibrium even after transient behavior.

Elimination of the bouncing phenomenon and elongation of the ball contact time in human side is performed by lowering stiffness values according to decreased cocontraction levels ( $t= 2.4$  to  $2.7$  sec), right after desired deviation from equilibrium position is ensured. This behavior is in accordance with previous studies on capabilities of the human body in minimization of soft-tissue vibrations and impact transition by means of increased damping or decreased stiffness (modified resonance frequency) within involved tissues [22]. These experimental results from the catching ball experiment demonstrate that the tele-impedance concept and the real time transfer of such adaptive mechanical properties to the slave robotic arm can permit to reach human-like performances in the ball reception stability and settling time. This behavior could be

considered as an adaptive change between optimum stiff and compliant values in order to improve stability (reduction of bouncing) while maintaining equilibrium position. Fig. 8 demonstrates the three ball reception quality indexes for the three different elastic profiles.

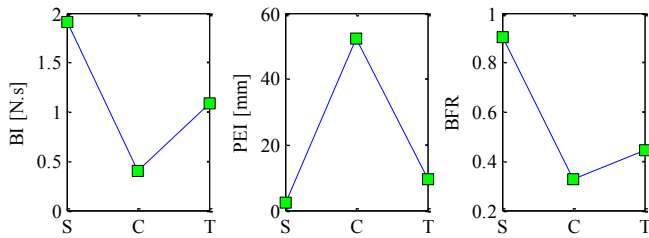


Fig. 8. Performance index plots over different elastic endpoint profiles (S: Stiff, C: Compliant and T: Tele-Impedance). Results show the optimized transient and steady state behavior compared to constant elastic profiles.

## V. DISCUSSIONS AND CONCLUSIONS

This work introduced the concept of Tele-Impedance, a method to effectively transfer task-efficient stiffness modifications of human, as a skillful master, to the robotic arm. Alternatively to position based or closed loop bilateral force reflecting teleoperation, the proposed approach augments the command sent to the robot by including both the position reference and the desired impedance profiles.

The impedance (stiffness) profile sent to the robot was derived in real time from the measurement of EMGs from eight muscles of the operator arm. A coactivation based index was proposed for the stiffness estimation of the human arm endpoint. This index were identified and calibrated by means of direct measurements of endpoint elastic profile by means of stochastic perturbations. The procedures used for the calibration of the model were introduced and the Tele-Impedance control concept was successfully demonstrated through a throwing ball reception task. In this Tele-Impedance setup, the position and the estimated stiffness of the human arm end point (wrist) were acquired and used to continuously command the Cartesian position and stiffness of the KUKA light weight arm. Performance indexes corresponding to the bouncing behavior of the ball, resulted force impacts and deviation of the end effector of KUKA from equilibrium position were recruited for further analysis of the proposed algorithm. The results confirmed the superior performance of the Tele-Impedance control as far as the overall reception behavior is concerned considering both transient and steady state responses (Fig. 8). We believe that the human-inspired modulation of the endpoint impedance during execution of tasks with significant dynamics variation inquiries can finally permit robots or assistive devices to reach high interaction performances, and also possibility of demonstrating a versatile and stable behavior even when interacting with environments with dynamic uncertainties.

## VI. ACKNOWLEDGEMENTS

This work is supported by the European Community, under grants FP7 ICT-287513 “SAPHARI”, FP7 ICT-

248587, “THE Hand Embodied”, and FP7 ICT- 270350 “ROBLOG”.

## REFERENCES

- [1] R. Osu, DW. Franklin, H. Kato, H. Gomi, K. Domen, T. Yoshioka, and M. Kawato, “Short- and long-term changes in joint co-contraction associated with motor learning as revealed from surface EMG”. *J Neurophysiol.* vol. 88, pp. 991–1004, 2002.
- [2] P.L. Gribble, L.I. Mullin, N. Cothros and A. Mattar, “Role of cocontraction in arm movement accuracy,” *J. Neurophysiol.*, vol. 89, pp. 2396–2405, 2003.
- [3] J. del R. Millán, F. Renkens, J. Mouriño, and W. Gerstner, “Non-invasive brain-actuated control of a mobile robot by human EEG,” *IEEE Trans. Biomed. Eng.*, vol. 51, no. 6, pp. 1026–1033, Jun. 2004.
- [4] C. Castellini and P. van der Smagt, “Surface EMG in advanced hand prosthetics”. *Biological Cybernetics*, 2006.
- [5] P. K. Artemiadis and K. J. Kyriakopoulos, “EMG-based position and force control of a robot arm: Application to teleoperation and orthosis,” in *Proceedings of IEEE/ASME AIM*, pp. 1–6, 2007.
- [6] D. W. Franklin, R. Osu, E. Burdet, M. Kawato, and T. E. Milner, “Adaptation to stable and unstable dynamics achieved by combined impedance control and inverse dynamics model,” *J. Neurophysiol.*, vol. 90, no. 5, pp. 3270–3282, 2003.
- [7] E. J. Perreault, R. F. Kirsch, and P. E. Crago, “Multijoint dynamics and postural stability of the human arm,” *Exp. Brain Res.*, vol. 157, pp. 507–517, 2004.
- [8] H. Gomi and R. Osu, “Task-Dependent Viscoelasticity of Human Multi joint Arm and Its Spatial Characteristics for Interaction with Environments”. *J Neurosci.*, vol. 18, pp. 8965–78, 1998.
- [9] M. Kawato, “Internal models for motor control and trajectory planning,” *Current Opinion Neurobiol.*, vol. 9, pp. 718–727, 1999.
- [10] A. Albu-Schäffer, Ch. Ott, and G. Hirzinger “A unified passivity-based control framework for position, torque and impedance control of flexible joint robots”, in *Int. Journal of Robotics Research*, vol. 26, no. 1, pp. 23–39, 2007.
- [11] A. Bicchi and G. Tonietti, “Fast and soft arm tactics: Dealing with the safety-performance trade off in robot arms design and control,” *IEEE Robotics and Automation Mag.*, vol. 11, no. 2, pp. 22–33, 2004.
- [12] A.Jafari, N.G. Tsagarakis, B. Vanderborcht, and Darwin Caldwell, “AwAS: a novel actuator with adjustable stiffness,” in the *Proceeding of IEEE/RSJ IROS*, pp. 4201–4206, 2010.
- [13] G. Tonietti, R. Schiavi, and A. Bicchi, “Design and control of a variable stiffness actuator for safe and fast physical human/robot interaction,” in *Robotics and Automation*, pp. 526–531, 2005.
- [14] T. B. Sheridan, “Space teleoperation through time delay: Review and prognosis,” *IEEE Trans. Robot. Autom.*, vol. 9, no. 5, pp. 592–606, 1993.
- [15] A. Eusebi and C. Melchiorri, “Force reflecting telemanipulators with timedelay: Stability analysis and control design,” *IEEE Trans. Robot. Autom.*, vol. 14, no. 4, pp. 635–640, Aug. 1998.
- [16] D. A. Lawrence, “Stability and transparency in bilateral teleoperation,” *IEEE Trans. Robot. Autom.*, vol. 9, no. 5, pp. 624–637, Oct. 1993.
- [17] N. Hogan, “Impedance control: An approach to manipulation,” *Trans. ASME, J. Dyn., Syst. Meas., Control*, vol. 107, pp. 1–24, Mar. 1985.
- [18] G. Schreiber, A. Stemmer, and R. Bischoff, “The Fast Research Interface for the KUKA Lightweight Robot”. In *IEEE ICRA*, 2010.
- [19] T. Tsuji, Y. Takeda, and Y. Tanaka, “Analysis of mechanical impedance in human arm movements using a virtual tennis system,” *Biological Cyber.*, vol. 91, no. 5, pp. 295–305, 2004.
- [20] P. L. Gribble and D. J. Ostry, “Compensation for loads during arm movements using equilibrium-point control,” *Exp. Brain Research*, no. 135, pp. 474–482, 2000.
- [21] E. Burdet, R. Osu, D. W. Franklin, T. E. Milner, and M. Kawato, “The central nervous system stabilizes unstable dynamics by learning optimal impedance,” *Nature*, vol. 414, no. 6862, pp. 446–449, 2001.
- [22] J. M. Wakeling, A. M. Liphardt, and B. M. Nigg, “Muscle activity reduces soft-tissue resonance at heel-strike during walking,” *J. Biomech.*, vol. 36, pp. 1761–1769, 2003.